Analysis of the shell thickness distribution on NaYF4/NaGdF 4 core/shell nanocrystals by EELS and EDS

ARTICLE *in* JOURNAL OF PHYSICAL CHEMISTRY LETTERS · FEBRUARY 2011

Impact Factor: 7.46 · DOI: 10.1021/jz101593g

4 AUTHORS:

Keith A Abel
University of Victoria
14 PUBLICATIONS **439** CITATIONS
SEE PROFILE

John-Christopher Boyer
Simon Fraser University
48 PUBLICATIONS **4,493** CITATIONS
SEE PROFILE

Carmen M. Andrei
McMaster University
22 PUBLICATIONS **249** CITATIONS
SEE PROFILE

Frank C J M van Veggel
University of Victoria
120 PUBLICATIONS **6,838** CITATIONS
SEE PROFILE

THE JOURNAL OF PHYSICAL CHEMISTRY Letters

pubs.acs.org/JPCL

Analysis of the Shell Thickness Distribution on $NaYF_4$/$NaGdF_4$ Core/Shell Nanocrystals by EELS and EDS

Keith A. Abel,[†] John-Christopher Boyer,[†] Carmen M. Andrei,[‡] and Frank C. J. M. van Veggel*[,†]

[†]Department of Chemistry, University of Victoria, Victoria, BC V8W 3V6, Canada, and [‡]Canadian Centre for Electron Microscopy, McMaster University, Hamilton, ON L8S 4L7, Canada

ABSTRACT The structure and chemical composition of the shell distribution on $NaYF_4$/$NaGdF_4$ core/shell nanocrystals have been investigated with scanning transmission electron microscopy (STEM), electron energy loss spectroscopy (EELS), and energy-dispersive X-ray spectroscopy (EDS). The core and shell contrast in the high-angle annular dark-field (HAADF) images combined with the EELS and EDS signals indicate that Gd is indeed on the surface, but for many of the particles, the shell growth was anisotropic.

SECTION Nanoparticles and Nanostructures

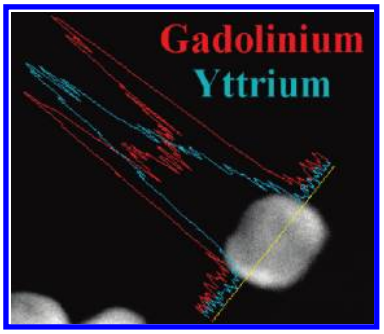

Upconverting lanthanide-based nanocrystals (NCs) are receiving considerable attention for their potential use as bioimaging probes.[1−3] The NCs absorb near-infrared (NIR) photons and emit higher energy photons, either in the UV−visible or NIR, which results in several advantages for bioimaging, such as deep tissue penetration and reduced autofluorescence. Recent work has suggested that they may be candidates for bimodal imaging by combining their emissions tunable across biological optical windows (by varying the dopant ions) and incorporating Gd^{3+} for magnetic resonance imaging (MRI) use.[4−8] In addition to applications as bioprobes, lanthanide-based NCs can be applied to a wide range of technologies such as optoelectronics, optical data storage, photochemistry, security labeling, and photodynamic therapy (PDT).[9−13]

To increase the overall photoluminescence (PL) efficiency of lanthanide-based NCs, core/shell heterostructures have been developed.[7,14−17] The large increases in PL have been attributed to protecting the luminescent dopant ions from quenching due to the surrounding environment (e.g., stabilizing ligands, solvent molecules, surface defects, etc.).[18] The core/shell structure is commonly inferred from optical measurements, but problems with this arise because luminescence measurements give no insight into the mechanism of shell growth or coverage. Standard transmission electron microscopy (TEM) is unable to differentiate between core and shell materials in lanthanide-based NCs because of similar material lattice constants and very little contrast difference between core and shell materials. We are not aware of any examples in the literature that show convincing contrast between core and shell materials for lanthanide-based NCs using standard TEM. Determination of the true structure of nanomaterials is imperative for their further development, and less common methods are thus required to characterize their structures. Recently, we reported on energy-dependent X-ray photoelectron spectroscopy (XPS) measurements performed with tunable synchrotron radiation on $NaYF_4$/$NaGdF_4$ NCs.[4] Hexagonal phase $NaYF_4$ is an efficient host material for upconverting lanthanide ions,[19] and $NaGdF_4$ has an excellent lattice match for shell growth with the added benefit of incorporating Gd^{3+} for MRI use. The XPS results show that Gd^{3+} resides predominantly on the surface of the NCs and provides, for the first time, concrete evidence of a core/shell structure. However, we were unable to draw conclusions on the overall thickness of the shells or whether isotropic shell growth had occured on individual $NaYF_4$ core NCs because the energy-dependent XPS method is an ensemble measurement. In this communication, we present high-angle annular dark-field (HAADF) images combined with electron energy loss spectroscopy (EELS) and energy-dispersive X-ray spectroscopy (EDS) data scanned across single particles that show unequivocally that the synthesized $NaYF_4$/$NaGdF_4$ NCs are indeed core/shell structures. However, we find that the synthetic procedure used in this report leads to anisotropic shell growth, which warrants further fine-tuning of the synthesis. The results presented herein are the first that show convincing contrast between core and shell materials for lanthanide-based NCs and should help to develop further these materials.

Scanning transmission electron microscopy (STEM), coupled to techniques such as EELS and EDS, is well suited to the characterization of materials with complex compositions on the nanoscale, providing both structural and chemical information.[20−22] Unlike conventional TEM, STEM operated in HAADF mode is far more sensitive to atomic number (Z) contrast, scaling proportionally to $\sim Z^2$.[23] In addition, the technique collects scattered electrons with an annular detector around the beam, allowing the main transmitted beam to pass through a magnetic prism that sorts the electrons according to their respective energies. EELS measures the change in the kinetic energy of the electrons after they have passed through the sample. The amount of energy

Received Date: November 24, 2010
Accepted Date: January 6, 2011
Published on Web Date: January 11, 2011

DOI: 10.1021/jz101593g | *J. Phys. Chem. Lett.* 2011, 2, 185–189

loss can be interpreted in terms of the electronic structure of the atoms under investigation, allowing for chemical mapping as the beam is scanned across the particle. Recent work on an ideal sample of layered perovskite Manganite has shown the high-resolution capability of the EELS technique with results on the atomic scale.[24] Alternatively, an X-ray detector can be used to measure EDS data and provide a supplementary method for determining chemical composition. However, beam damage to nanomaterials, caused by the long scan times required for EELS and in particular EDS, is still a challenge in the field and a limitation in some cases.

The synthesis and standard characterization (e.g., XRD, EDS, TEM, XPS, etc.) of the $NaYF_4/NaGdF_4$ NCs used in this report have previously been described in detail.[4] Herein, we focus on the structural and compositional analysis of the shell distribution using a combination of EELS and EDS in STEM mode. For simplicity, we chose to exclude dopant ions and focus on characterizing the overall structure of the NC matrix. The high-resolution (HR) HAADF images were acquired with an FEI Titan 80-300 TEM, equipped with image and probe aberration correctors. Standard HAADF images combined with EELS or EDS data were acquired with a FEI Titan 80-300 TEM equipped with image corrector, operated at 300 kV. The system is equipped with a Gatan image filter (GIF). EELS measurements were performed in STEM mode with a convergence angle of 8 mrad and a collection angle of 15 mrad. The energy resolution was ~0.7 eV. All acquisition and data analysis were carried out using Digital Micrograph software, with spectrum imaging scripts provided by Gatan. We prepared STEM samples by depositing the NCs from tetrahydrofuran (THF) directly onto ultrathin carbon film supported on a copper grid. In addition to the standard washing procedure employed during NC preparation, samples were plasma cleaned for 20 s to remove hydrocarbon contamination and then loaded immediately into the microscope. An O_2/H_2 (O_2 99.-999 % and H_2 99.995 % purity) gas mixture of 27.5 standard cubic centimeter (sccm) O_2 and 6.4 sccm H_2 was utilized during the plasma cleaning. For EELS, the acquisition time was 0.5 s/pixel, and the pixel size was ~0.5 nm. The time per frame was 0.5 s for EDS with ~4300 frames (i.e., total acquisition time of ~36 min).

A low-magnification standard HAADF image of the core/shell NCs is shown in the Supporting Information (Figure S1). The average size of the core/shell NCs was determined to be 23 ± 3 nm in diameter by averaging over the long and short axes and is comparable to our previously reported result.[4] The original $NaYF_4$ core NCs had a diameter of 16 ± 1 nm. The increase in overall size suggests successful growth of $NaGdF_4$ onto the $NaYF_4$ cores, with an average shell thickness of 3.5 nm. We note that some smaller particles are present that are individually nucleated $NaGdF_4$ NCs (Figure S2 of the Supporting Information), and these have been ignored in the average diameter calculation. Careful optimization of the synthetic procedure would likely result in the absence of any individually nucleated $NaGdF_4$ NCs. Alternatively, they could be removed by centrifugation methods. Figure 1 is an HR-HAADF image, and clear contrast between the core (dark) and shell (bright) materials can be seen. The contrast is attributed to the much larger atomic number of Gd (Z = 64) compared with Y (Z = 39) and demonstrates the power of this technique. For standard TEM, other than an increase in average particle size, there would be no indication of shell growth for these materials.

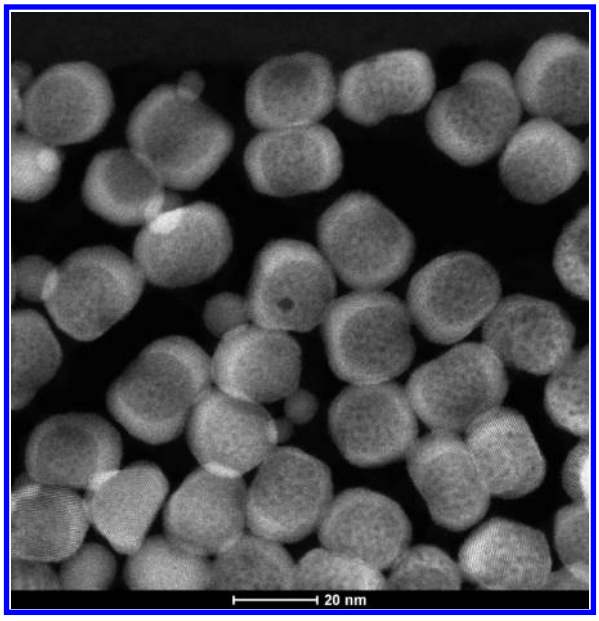

Figure 1. Low-magnification HR-HAADF image of $NaYF_4/NaGdF_4$ core/shell NCs. Both core (dark) and shell (bright) materials are visible in the image.

Figure 2 shows higher magnification HR-HAADF images of typical $NaYF_4/NaGdF_4$ core/shell NCs in different crystal orientations. The inset of Figure 2a is a fast Fourier transform (FFT) of the HAADF image that clearly shows the hexagonal lattice structure. The NC in Figure 2b has a lattice spacing of ~0.52 nm corresponding to the $(10\bar{1}0)$ plane and shows increased growth perpendicular to the plane, that is, the [0001] direction (discussed further below).

As has been pointed out previously, HAADF images provide qualitative information and cannot be used to determine chemical composition because both atomic number and thickness may influence the contrast.[22] For this reason, it was imperative to combine EELS data with this technique. EELS line scans were acquired across either a single particle or two neighboring particles. Figure 3a,b shows HAADF images of typical isolated core/shell NCs, with the corresponding EELS spectra of the Gd $N_{4,5}$ edge at 140 eV shown in Figure 3c,d, respectively. The intensity of the Gd signal changes with position across the particle. At the edges of the NCs, the Gd signal is significantly larger than at the center. For a spherical NC with a core/shell structure, the EELS signal of the shell material is expected to be proportional to the thickness of the shell in the z direction (i.e., normal to the plane of incidence). The thickness of the shell at the edge of a core/shell NC is larger than that at the center, and correspondingly, the EELS signal is expected to be larger.[22] Figure 3 clearly shows that the measured particles are core/shell NCs with Gd definitely located in the shell.

Unfortunately, the Y $M_{4,5}$ edge at 157 eV was close to a delayed Gd edge, and the signal could not clearly be resolved;

DOI: 10.1021/jz101593g | J. Phys. Chem. Lett. 2011, 2, 185–189

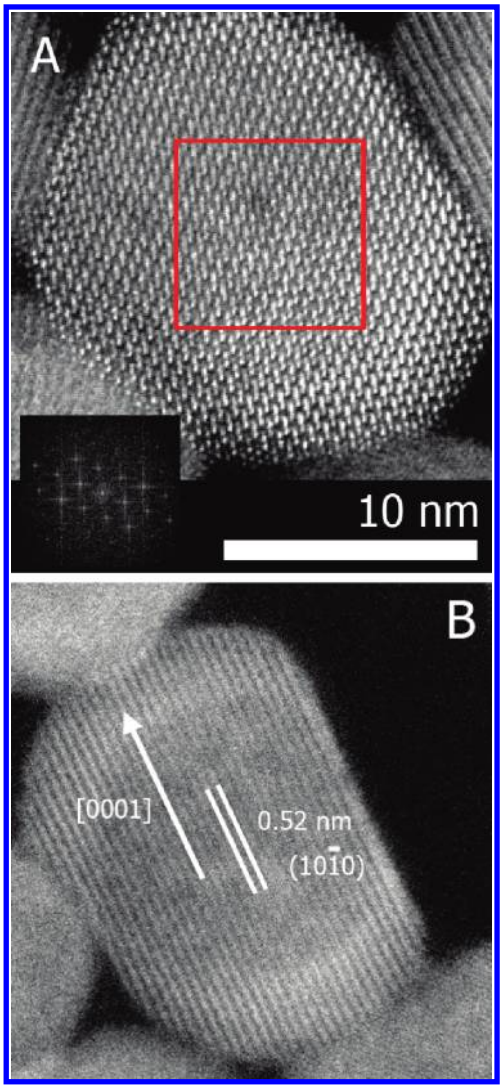

Figure 2. (a) HR-HAADF image of a $NaYF_4/NaGdF_4$ core/shell NC; the inset is the corresponding FFT image showing the hexagonal lattice structure. (b) HR-HAADF image of a $NaYF_4/NaGdF_4$ core/shell NC showing faster growth in the [0001] direction.

therefore, we were unable to show that Y was located at the center of the NCs using EELS. We also checked the Y edges at 300, 312, and 394 eV, but these are minor edges, and there was no clear signal present. Therefore, we performed line scans on single particles using EDS instead of EELS to confirm that Y is indeed located at the center of the particle. An example of an EDS line scan across a single particle is shown in Figure 4.

The EDS data clearly show that Y is located in the core of the particle and Gd is at the edges, supporting a $NaYF_4/NaGdF_4$ core/shell structure. The acquisition of an EELS line scan was ~1 min, whereas the EDS acquisition took ~36 min. Hence, all HAADF images after an EDS line scan showed noticeable beam damage (Figure S3 of the Supporting Information) and also some sample drift. The drift was corrected by the Inca acquisition software. Therefore, we continued with EELS measurements to reduce data acquisition times and beam damage.

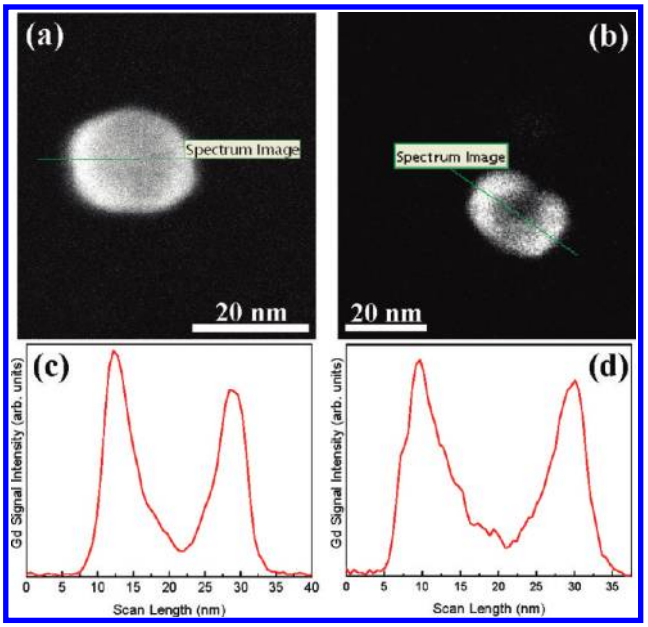

Figure 3. (a,b) HAADF images of single $NaYF_4/NaGdF_4$ core/shell NCs and the corresponding (c,d) EELS line scans showing Gd residing predominantly in the shell.

Further EELS analysis on more than 30 particles found that the shell layer was not uniformly distributed on all particles, which is consistent with the image contrast in the HR-HAADF images shown in Figure 1. Although most were core/shell, some of the particles had thick shells on parts of the particle and much thinner shell thickness on the other sides. An example of anisotropic shell growth is shown in Figure 5a,b, with EELS data shown in Figure 5c,d (further STEM-EELS measurements are shown in Figure S4 of the Supporting Information).

These results suggest that certain facets of the core are more reactive than others, leading to nonuniform shell thicknesses during growth. This is a surprising result considering the excellent lattice match between the core and shell materials (β-$NaYF_4$ JCPDS-PDF no. 016-0334 and β-$NaGdF_4$ JCPDS-PDF no. 027-0699). A detailed examination of the HR-HAADF images revealed that shell growth occurs more slowly on the (10$\bar{1}$0) prismatic planes and more quickly on the (0001) top/bottom planes (example shown in Figure 2b). It has been noted in the past that carboxylic-acid-based ligands have a tendency to direct growth toward different planes of the hexagonal $NaYF_4$ lattice.[25] Li and Zhang found that the concentration of oleic acid ligand affected the growth rates of hexagonal phase $NaYF_4$ NCs in different directions.[19] It is possible that in our case the oleic acid ligand used in the synthesis of the core/shell NCs dictates preferential (or inhibited) growth along certain planes of the NCs, and thin or even incomplete shell growth results. We also note that Yan and coworkers showed very different growth behaviors for $NaYF_4$ and $NaGdF_4$ NCs.[26] For instance, in oleic acid/octadecene, $NaYF_4$ requires high-temperatures to form the hexagonal phase, but $NaGdF_4$ easily formed the hexagonal phase because of a relatively low energy barrier resulting in irregular particles (for short reaction times) or nanorods (with increasing reaction time). The preferred anisotropic growth of $NaGdF_4$

DOI: 10.1021/jz101593g | J. Phys. Chem. Lett. 2011, 2, 185–189

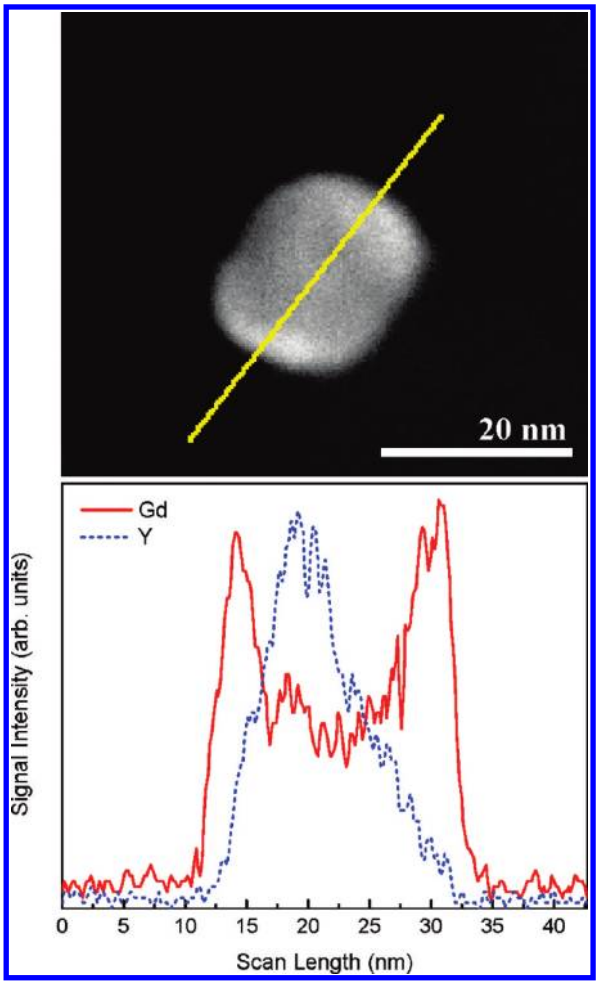

Figure 4. EDS line scan across a single $NaYF_4/NaGdF_4$ core/shell NC showing Y in the core of the particle and Gd located in the shell.

may be involved in the uneven shell growth we observe. We also speculate that defects located on the surface of the $NaYF_4$ NCs may play a role in the nucleation of the shell and ultimately lead to anisotropic shell growth in some particles. Understanding the exact mechanism is beyond the scope of this Letter but would certainly be of interest to the scientific community. STEM simulations are underway to understand better the relation between core and shell as well as shell growth and coverage. Considering the impact shell growth has on the luminescence efficiency, optimization of synthetic parameters to increase core coverage on every NC could be tremendously beneficial for further improving the optical properties of luminescent lanthanide dopant ions. However, because of the large number of synthetic parameters involved, improvements will likely come from substantial trial and error experimentation. It is important to note that although shell growth was not isotropic, in many cases, the resulting core/shell particles were spherical and under standard TEM could have been misinterpreted as core/shell NCs with uniform shell thicknesses.

Previous work using energy-dependent XPS shows an increase in the Y^{3+}/Gd^{3+} ratio at increasing kinetic energies.[4]

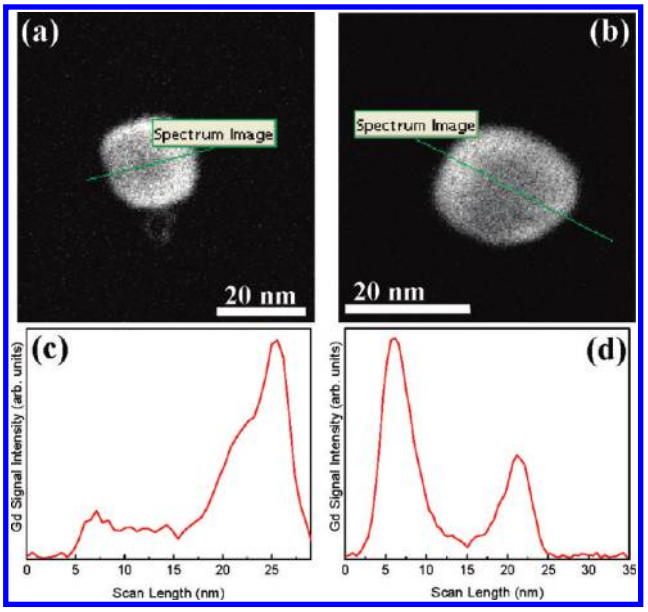

Figure 5. (a,b) HAADF images of single $NaYF_4/NaGdF_4$ core/shell NCs and the corresponding (c,d) EELS line scans showing nonuniform shell distribution.

The ratio increase is caused by the screening of the Y^{3+} intensity by the surrounding Gd^{3+} atoms at low kinetic energies. Alloys are expected to show constant intensity ratios with increasing kinetic energies. If the starting core size is known and a sharp interface between core and shell materials is assumed, then the energy-dependent XPS data can be modeled to obtain the shell thickness, as has been pointed out in other reports.[27−30] However, the data presented herein show that the shell distributions vary; therefore, the XPS data can only be taken as an overall average. Varied shell thicknesses as well as individually nucleated $NaGdF_4$ NCs will decrease the slope of the Y^{3+}/Gd^{3+} ratio in the XPS data. Although STEM-EELS is more straightforward compared with XPS work at a synchrotron, we note that EELS is most suited for light elements and the resolution is often not high enough for very small particles (or thin shells); therefore, techniques such as energy-dependent XPS remain very useful. Furthermore, the electron dosage required for EDS analysis on single particles in many instances is too high and destroys the NCs before useful information is obtained.

In conclusion, utilizing both EELS and EDS in STEM mode, we have shown that the synthesized $NaYF_4/NaGdF_4$ NCs do in fact have a core/shell structure. However, we have also shown that complete and uniform shell growth does not occur on all of the NCs. Further improvements in synthetic procedure will likely improve shell quality. For instance, a recently reported procedure on $NaYF_4/NaGdF_4$ NCs showed improvements in overall monodispersity and possible isotropic shell growth, but no direct evidence of a core/shell structure was provided.[31] We suggest that new synthetic procedures in the field undergo similar experiments to determine accurately structural information.

SUPPORTING INFORMATION AVAILABLE Supporting Figures described in the text, additional HAADF images, and EELS

DOI: 10.1021/jz101593g | J. Phys. Chem. Lett. 2011, 2, 185–189

data. This material is available free of charge via the Internet at http://pubs.acs.org.

AUTHOR INFORMATION

Corresponding Author:

*To whom correspondence should be addressed. E-mail: fvv@uvic.ca.

ACKNOWLEDGMENT This work was supported by the Natural Sciences and Engineering Research Council (NSERC) of Canada, the Canada Foundation for Innovation (CFI), and the British Columbia Knowledge Development Fund (BCKDF).

REFERENCES

(1) Mader, H. S.; Kele, P.; Saleh, S. M.; Wolfbeis, O. S. Upconverting Luminescent Nanoparticles for use in Bioconjugation and Bioimaging. *Curr. Opin. Chem. Biol.* **2010,** *14*, 582–596.

(2) Wang, F.; Banerjee, D.; Liu, Y.; Chen, X.; Liu, X. Upconversion Nanoparticles in Biological Labeling, Imaging, and Therapy. *Analyst* **2010,** *135*, 1839–1854.

(3) Wang, F.; Liu, X. G. Recent Advances in the Chemistry of Lanthanide-Doped Upconversion Nanocrystals. *Chem. Soc. Rev.* **2009,** *38*, 976–989.

(4) Abel, K. A.; Boyer, J.-C.; van Veggel, F. C. J. M. Hard Proof of the $NaYF_4$/$NaGdF_4$ Nanocrystal Core/Shell Structure. *J. Am. Chem. Soc.* **2009,** *131*, 14644–14645.

(5) Aime, S.; Botta, M.; Terreno, E. Gd(III)-Based Contrast Agents for MRI. *Adv. Inorg. Chem.* **2005,** *57*, 173–237.

(6) Evanics, F.; Diamente, P. R.; van Veggel, F. C. J. M.; Stanisz, G. J.; Prosser, R. S. Water-Soluble GdF_3 and GdF_3/LaF_3 Nanoparticles-Physical Characterization and NMR Relaxation Properties. *Chem. Mater.* **2006,** *18*, 2499–2505.

(7) Park, Y. I.; Kim, J. H.; Lee, K. T.; Jeon, K.-S.; Na, H. B.; Yu, J. H.; Kim, H. M.; Lee, N.; Choi, S. H.; Baik, S.-I.; et al. Nonblinking and Nonbleaching Upconverting Nanoparticles as an Optical Imaging Nanoprobe and T1 Magnetic Resonance Imaging Contrast Agent. *Adv. Mater.* **2009,** *21*, 4467–4471.

(8) Wang, F.; Han, Y.; Lim, C. S.; Lu, Y.; Wang, J.; Xu, J.; Chen, H.; Zhang, C.; Hong, M.; Liu, X. Simultaneous Phase and Size Control of Upconversion Nanocrystals through Lanthanide Doping. *Nature* **2010,** *463*, 1061–1065.

(9) Carling, C.-J.; Boyer, J.-C.; Branda, N. R. Remote-Control Photoswitching using NIR Light. *J. Am. Chem. Soc.* **2009,** *131*, 10838–10839.

(10) Carling, C.-J.; Nourmohammadian, F.; Boyer, J.-C.; Branda, N. R. Remote-Control Photorelease of Caged Compounds using Near-Infrared Light and Upconverting Nanoparticles. *Angew. Chem., Int. Ed.* **2010,** *49*, 3782–3785.

(11) Chatterjee, D. K.; Yong, Z. Upconverting Nanoparticles as Nanotransducers for Photodynamic Therapy in Cancer Cells. *Nanomedicine* **2008,** *3*, 73–82.

(12) Qian, H. S.; Guo, H. C.; Ho, P. C.-L.; Mahendran, R.; Zhang, Y. Mesoporous-Silica-Coated Up-Conversion Fluorescent Nanoparticles for Photodynamic Therapy. *Small* **2009,** *5*, 2285–2290.

(13) Zhang, P.; Steelant, W.; Kumar, M.; Scholfield, M. Versatile Photosensitizers for Photodynamic Therapy at Infrared Excitation. *J. Am. Chem. Soc.* **2007,** *129*, 4526–4527.

(14) Boyer, J.-C.; Gagnon, J.; Cuccia, L. A.; Capobianco, J. A. Synthesis, Characterization, and Spectroscopy of $NaGdF_4$:Ce^{3+}, Tb^{3+}/$NaYF_4$ Core/Shell Nanoparticles. *Chem. Mater.* **2007,** *19*, 3358–3360.

(15) Mai, H.-X.; Zhang, Y.-W.; Sun, L.-D.; Yan, C.-H. Highly Efficient Multicolor Up-Conversion Emissions and their Mechanisms of Monodisperse $NaYF_4$:Yb,Er Core and Core/Shell-Structured Nanocrystals. *J. Phys. Chem. C* **2007,** *111*, 13721–13729.

(16) Qian, H.-S.; Zhang, Y. Synthesis of Hexagonal-Phase Core-Shell $NaYF_4$ Nanocrystals with Tunable Upconversion Fluorescence. *Langmuir* **2008,** *24*, 12123–12125.

(17) Yi, G.-S.; Chow, G.-M. Water-Soluble $NaYF_4$:Yb,Er(Tm)/$NaYF_4$/Polymer Core/Shell/Shell Nanoparticles with Significant Enhancement of Upconversion Fluorescence. *Chem. Mater.* **2007,** *19*, 341–343.

(18) Wang, F.; Wang, J.; Liu, X. Direct Evidence of a Surface Quenching Effect on Size-Dependent Luminescence of Upconversion Nanoparticles. *Angew. Chem., Int. Ed.* **2010,** *49*, 7456–7460.

(19) Li, Z.; Zhang, Y. An Efficient and User-Friendly Method for the Synthesis of Hexagonal-Phase $NaYF_4$:Yb, Er/Tm Nanocrystals with Controllable Shape and Upconversion Fluorescence. *Nanotechnology* **2008,** *19*, 345606.

(20) Rosenthal, S. J.; McBride, J.; Pennycook, S. J.; Feldman, L. C. Synthesis, Surface Studies, Composition and Structural Characterization of CdSe, Core/Shell and Biologically Active Nanocrystals. *Surf. Sci. Rep.* **2007,** *62*, 111–157.

(21) Sanchez, S. I.; Small, M. W.; Zuo, J.; Nuzzo, R. G. Structural Characterization of Pt-Pd and Pd-Pt Core-Shell Nanoclusters at Atomic Resolution. *J. Am. Chem. Soc.* **2009,** *131*, 8683–8689.

(22) Yu, Z.; Guo, L.; Du, H.; Krauss, T.; Silcox, J. Shell Distribution on Colloidal CdSe/ZnS Quantum Dots. *Nano Lett.* **2005,** *5*, 565–570.

(23) Sanchez, S. I.; Small, M. W.; Sivaramakrishnan, S.; Wen, J.-g.; Zuo, J.-M.; Nuzzo, R. G. Visualizing Materials Chemistry at Atomic Resolution. *Anal. Chem.* **2010,** *82*, 2599–2607.

(24) Kimoto, K.; Asaka, T.; Nagai, T.; Saito, M.; Matsui, Y.; Ishizuka, K. Element-Selective Imaging of Atomic Columns in a Crystal using STEM and EELS. *Nature* **2007,** *450*, 702–704.

(25) Li, C.; Quan, Z.; Yang, J.; Yang, P.; Lin, J. Highly Uniform and Monodisperse β-$NaYF_4$:Ln^{3+} (Ln = Eu, Tb, Yb/Er, and Yb/Tm) Hexagonal Microprism Crystals: Hydrothermal Synthesis and Luminescent Properties. *Inorg. Chem.* **2007,** *46*, 6329–6337.

(26) Mai, H.-X.; Zhang, Y.-W.; Si, R.; Yan, Z.-G.; Sun, L.-d.; You, L.-P.; Yan, C.-H. High-Quality Sodium Rare-Earth Fluoride Nanocrystals: Controlled Synthesis and Optical Properties. *J. Am. Chem. Soc.* **2006,** *128*, 6426–6436.

(27) Borchert, H.; Haubold, S.; Haase, M.; Weller, H.; McGinley, C.; Riedler, M.; Miller, T. Investigation of ZnS Passivated InP Nanocrystals by XPS. *Nano Lett.* **2002,** *2*, 151–154.

(28) Borchert, H.; Talapin, D. V.; McGinley, C.; Adam, S.; Lobo, A.; Castro, A. R. B. d.; Möller, T.; Weller, H. High Resolution Photoemission Study of CdSe and CdSe/ZnS Core-Shell Nanocrystals. *J. Chem. Phys.* **2003,** *119*, 1800–1807.

(29) Kömpe, K.; Borchert, H.; Storz, J.; Lobo, A.; Adam, S.; Möller, T.; Haase, M. Green-Emitting $CePO_4$:Tb/$LaPO_4$ Core-Shell Nanoparticles with 70 % Photoluminescence Quantum Yield. *Angew. Chem., Int. Ed.* **2003,** *42*, 5513–5516.

(30) McGinley, C.; Borchert, H.; Talapin, D. V.; Adam, S.; Lobo, A.; de Castro, A. R. B.; Haase, M.; Weller, H.; Möller, T. Core-Level Photoemission Study of the InAs/CdSe Nanocrystalline System. *Phys. Rev. B* **2004,** *69*, 045301.

(31) Guo, H.; Li, Z.; Qian, H.; Hu, Y.; Muhammad, I. N. Seed-Mediated Synthesis of $NaYF_4$:Yb, Er/$NaGdF_4$ Nanocrystals with Improved Upconversion Fluorescence and MR Relaxivity. *Nanotechnology* **2010,** *21*, 125602.

DOI: 10.1021/jz101593g | *J. Phys. Chem. Lett.* **2011,** *2*, 185–189